

## Algorithms for EOR imaging using crosshole seismic data: an experiment with scale model data

R. Gerhard Pratt<sup>a</sup>, Li Quan<sup>b</sup>, Ben C. Dyer<sup>c</sup>, Neil R. Goult<sup>d</sup> and M.H. Worthington<sup>b</sup>

<sup>a</sup>*Department of Physics, University of Toronto, Toronto, M5S 1A7, Canada*

<sup>b</sup>*Department of Geology, Imperial College of Science, Technology and Medicine, London, SW7 2BP, UK*

<sup>c</sup>*Tomographic Imaging Ltd., 33 Birnam Rd., London, N4 3LJ, UK*

<sup>d</sup>*Department of Geological Sciences, University of Durham, South Rd., Durham, DH1 3LE, UK*

(Received September 28, 1990; accepted after revision April 4, 1991)

### ABSTRACT

Pratt, R.G., Quan, L., Dyer, B.C., Goult, N.R. and Worthington, M.H., 1991. Algorithms for EOR imaging using crosshole seismic data: an experiment with scale model data. In: B.K. Sternberg, M.M. Poulton and M.J. Sully (Editors), *Int. Symp. on Borehole Geophysics: Petroleum, Hydrology, Mining and Engineering Applications*. *Geoexploration*, 28: 193–220.

Seismic velocities are influenced by many enhanced oil recovery (EOR) techniques. The crosshole seismic survey is well suited to the mapping of injection fluids or fracture patterns following reservoir stimulation. Both traveltime tomography and wave-equation techniques can be used to monitor and map changes in the seismic velocities, given pre-stimulation and post-stimulation crosshole seismic data.

In order to evaluate algorithms for EOR mapping using crosshole seismic surveys, data were obtained from a scale model of a crosshole seismic survey. The epoxy resin model contained simulated geological structures with strong velocity contrasts. Two versions of the same model were constructed, both with and without a simulated “flood” zone of a known geometry. Traveltime tomography and tow wave-equation algorithms, the inverse generalized Radon transform (inverse GRT) and frequency-domain wave-equation imaging, were used to attempt to locate the extent and velocities of the perturbation.

The results of this experiment show that traveltime tomography suffices to locate the flood zone and to determine the magnitude of the velocity perturbations. However, images that resolve the geometry of the flood zone were only obtained when the full waveform was utilized, using either the inverse GRT or frequency-domain wave-equation imaging. In this experiment the best images of the flood zone were obtained using frequency-domain wave-equation imaging. This result is due to the (realistic) complexity of the model, which supports wave types not accounted for by the acoustic ray approximation used in tomography and in the inverse GRT.

Image quality depends on how the input data to the full waveform schemes are generated. For the inverse GRT the change in interface reflectivities due to the flood zone could be detected using pre-processed, “scattered” wave fields as input data. However, better images of the geometry of the flood zone were produced when the input data consisted of “difference” wave fields (the subtraction of pre-flood data from post-flood data). Although the inverse GRT contains an “obliquity factor” that will normally ensure a high image quality, a further result of the experiment is that the obliquity factor in the inverse GRT needed to be suppressed to image the flood zone directly from the difference data.

## INTRODUCTION

Enhanced oil recovery (EOR) is a topic of increasing interest to the petroleum extraction industry. EOR can be achieved by altering factors that determine the production rates of hydrocarbons. Two possibilities are (1) the injection of fluids to increase differential pressures or reduce viscosity, and (2) the enhancement of permeabilities by induced fracturing of the reservoir rocks. It is of interest to learn about the areal extent of the injection fluids or fracture patterns following reservoir stimulation, in order to facilitate the planning of production strategies. Geophysical surveys that provide such information are a subset of a large number of possible EOR monitoring methods.

The various merits of current EOR monitoring techniques are reviewed by Wayland and Leighton (1985). Among the methods discussed are pressure testing, tracer analysis and seismic methods. The use of seismology to monitor oil reservoirs is also discussed by Nur (1982) and Kretzschmar et al. (1982). Seismic velocities are often influenced by EOR techniques, thus the seismic survey is well suited to this application. The attraction of the seismic method to monitor EOR lies in the ability to map formation parameters and, by repeated application, to monitor changes in these parameters. The success of monitoring techniques will depend on the magnitudes of the velocity perturbations introduced. Toksöz et al. (1976) have estimated that CO<sub>2</sub> flooding may cause compressional velocity changes of a few percent (although this depends on the nature of the reservoir). Steam flooding and in-situ combustion can induce much greater velocity changes, due to the dependence of seismic velocities on temperatures (Wang and Nur, 1988). The crosshole seismic survey is particularly suited to the problem. Recently Justice et al. (1989) successfully used crosshole seismic traveltimes tomography to map the progress of steam injection floods. Similarly, Bregman et al. (1989b) used the technique to map in-situ combustion fronts.

This article will deal specifically with the image processing of crosshole seismic survey data. We seek herein to provide a controlled experiment that will allow the objective comparison of several algorithms. The experiment consists of a simulation of a crosshole seismic EOR monitoring survey, carried out in an ultrasonic modelling tank. We built two similar models that differed only in the velocities in a specific "flood zone". Scale crosshole surveys were carried out in both models, and the resultant data were processed using three different imaging algorithms. The three algorithms used were traveltimes tomography, the inverse generalized Radon transform (inverse GRT) (Miller et al., 1987) and frequency-domain wave-equation imaging (Pratt and Worthington, 1990).

Processing algorithms can be broadly divided into arrival-time analysis (traveltimes tomography) and wave-equation techniques. Traveltimes tomography generally operates on only the first arrival times to produce a map of

the velocities between boreholes. Wave-equation techniques are required to account for (and make use of) scattering and dispersion of the seismic wave; these effects are usually ignored when performing traveltime tomography. Wave equation techniques can be likened to the focussing algorithms employed in the (pre-stack) migration of surface seismic data. As in migration, wave-equation processes operate on the full recorded wave yield to field images of geological discontinuities (reflectors and scatterers) in the interwell region.

Traveltime tomography with applications to crosshole seismic data has an extensive literature associated with it. McMechan (1983), Worthington (1984) and Wong et al. (1987) all provide comprehensive reviews. The first application of the method to petroleum exploration and development appeared in 1971 (Bois et al., 1971). Examples of the application of traveltime tomography to crosshole data are more prevalent than examples of the application of wave-equation techniques. Exceptions include Chang and McMechan (1986), Lo et al. (1988), Pratt and Worthington (1988), Hu et al. (1988) and Beydoun et al. (1989).

Wave-equation techniques can be subdivided into imaging algorithms and inversion algorithms. The distinction between these approaches lies in the objectives of the algorithm. Imaging algorithms seek to focus scattered waves at their point of origin in the geophysical model. Inversion algorithms are more ambitious; an inversion algorithm seeks to identify where the geophysical model is in error and to provide an estimate of the corrections that are required. In general many iterations of an inversion technique will be required to achieve complete convergence. Nonetheless, often useful results can be obtained from a first iteration only, provided that the starting model is a good representation of the gross velocity variations. Fortunately, traveltime tomography furnishes appropriately smooth starting models. With smooth starting models the model errors are concentrated at velocity discontinuities, and thus the migration and inversion approaches tend to resemble each other. The combined use of traveltime tomography and wave-equation imaging has been shown by Pratt and Gouly (1991) to be an effective approach.

Both the inverse GRT and frequency-domain wave-equation imaging are mathematically formulated as inversion methods. However, the inverse GRT is a linearized inversion method and converges in a single iteration for linear problems. Frequency-domain wave-equation imaging is a non-linear inversion method requiring multiple iterations to achieve convergence, even for linear problems (for a full discussion and an illustration of this point, see Pratt and Worthington, 1990). In this paper we apply only a single iteration of each of these methods. Further iterations require subtracting *modelled* waveforms from observed waveforms. We argue that, given contemporary se-

ismic modelling methods, this subtraction would be dominated by modelling errors (even for the relatively simple model considered here). Therefore, no iterative inversion method can (yet) be carried beyond the first iteration.

In some respects the imaging of alterations to petrophysical parameters is a less difficult problem than the mapping of static geological structure. In principle, in EOR imaging, the seismic experiment can be carried out twice and any differences in the recorded wave fields should be attributable to alterations due to EOR stimulation. We shall refer to the result of such a subtraction of datasets as a "difference" wave field. In practice, operational constraints may cause the difference wave field to be contaminated by other effects, such as coupling inconsistencies or source signature variations. However, traveltimes are relatively insensitive to these effects, and therefore traveltimes inversion can be considered to be quite robust.

Without the existence of a pre-stimulation dataset, wave-equation techniques require that crosshole data be extensively pre-processed. The primary objective of the pre-processing is to separate directly arriving (high-amplitude) components in the wave fields from the low-amplitude scattered components. We refer to the two components as the "direct" wave field and the "scattered" wave field. The scattered wave reaches the receivers indirectly, having been scattered, reflected, diffracted or otherwise perturbed from the direct wave paths by geological anomalies. The imaging process serves to map events in the scattered wave field onto the scattering locations in the image. The separation of the two wave fields is essential, since the direct wave field is re-focused by wave-equation methods everywhere in the image (Chang and McMechan, 1986). This leads to an unacceptable corruption to the images if the direct wave field is not removed beforehand. It will be shown that the two approaches to pre-processing, leading to either a difference wave field or a scattered wave field, result in very different images.

Since wave-equation techniques require a solution to the forward problem, a further distinction between wave-equation techniques can be made according to the forward modelling methods that are implemented. For generality and computational efficiency, the method of choice is ray tracing (Chapman, 1978). However, ray theory has its limitations. In particular, the more complex a model is the more difficult it will be to obtain a solution to the ray equation linking a given pair of points. When model becomes complex (and we would like our models to reflect the complexity of the real world) a better technique is the method of finite differences (Kelly et al., 1976). The method of finite differences has the advantage of automatically generating all wave types and can handle completely general velocity distributions, although this generality comes at a significant computational cost. In this paper, the inverse GRT algorithm employs ray tracing to forward model the data, whereas wave-equation imaging employs frequency-domain finite differences.

SCALE MODEL DESCRIPTION

In order to provide suitable data to evaluate imaging methods, two cross-hole seismic surveys were simulated in the ultrasonic seismic modeling system at University of Durham (Sharp et al., 1985). The epoxy resin models each consisted of a layered structure with increasing velocities from top to

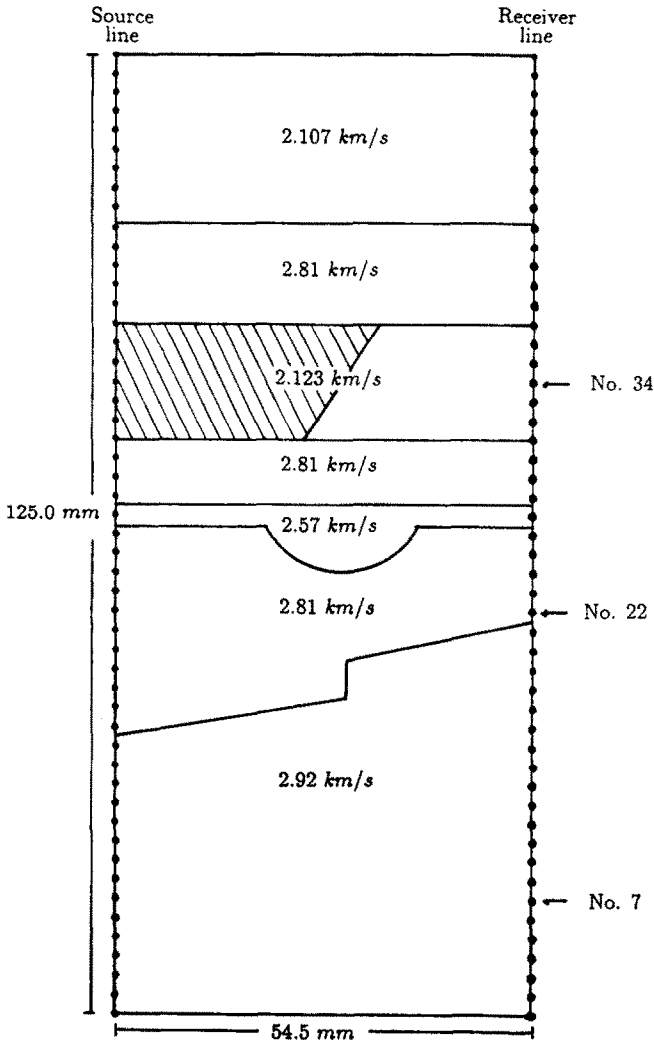


Fig. 1. Schematic of the layered epoxy resin scale models used to simulate the crosshole surveys. A total of 51 source positions were used and waveforms were recorded at 51 receiver positions. The models extended vertically beyond the limits shown here by 37 mm in either direction, and by 87 mm in both directions out of the plane. Two models were built, in the second model a lower velocity material was used in the cross-hatched region in the figure.

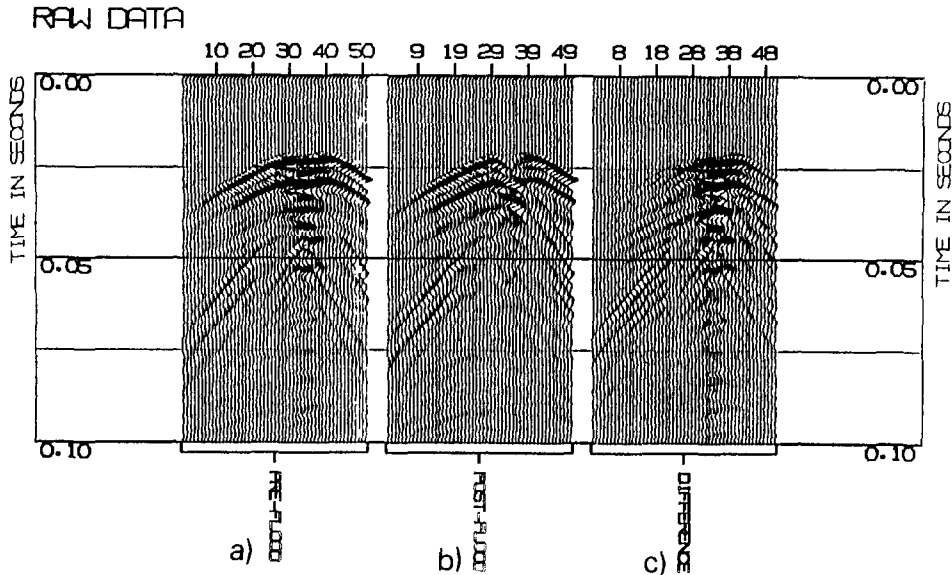


Fig. 2. Raw data from a single common receiver gather (No. 34) of the ultrasonic scale model experiment. (a) "Pre-flood" data, (b) "post-flood" data, and (c) the difference wave field obtained by subtracting the pre-flood data from the post-flood data. Numbers on the horizontal axes refer to the source numbers (see Fig. 1).

bottom (see Fig. 1). Two anomalies were included that simulated (i) a dipping layer with a vertical discontinuity, and (ii) a channel that cut into the center of one of the horizontal beds. Nominal velocities ranged from 2.123 km/s in one low velocity "reservoir" layer to 2.92 km/s at the bottom. Two models were prepared, the second identical to the first except for the inclusion of a simulated flood zone in the reservoir layer. The nominal velocity of the flood zone was 2.107 km/s.

The models were submerged in water and, by positioning ultrasonic piezoelectric transducers at the left and right edges of the models, transmission experiments were carried out using 51 source positions. Waveforms from each source position were recorded at 51 receiver positions, giving a total of 2601 traces in each survey. The bandwidth of the transmitted data lies between 200 and 500 kHz.

The model can be scaled up to realistic dimensions by multiplying distances and times by a factor of 1000 (millimetres become metres and microseconds become milliseconds). Thus the experiment simulated a cross-hole survey in which the interwell spacing was 54.5 m, and the depth interval was 125 m. The scaled frequencies of the recorded data ranged between 200 and 500 Hz. A typical common receiver gather of the data is shown in Fig. 2a.

## ALGORITHMS

This section will introduce the three approaches used to form images from the data from the scale model experiment described in the previous section.

*Traveltime tomography*

Traveltime tomography is conceptually simple, but has proven to be a difficult technique to implement effectively in practice. The basis of traveltime tomography is the linear equation system:

$$\delta T_k = \left( \frac{\partial T}{\partial U} \right)_{ki} \delta U_i \quad (1)$$

(summation notation used), where  $\delta T_k$  is the differential traveltime (differences between observed and modelled times) for the  $k$ th seismic trace and  $\delta U_i$  is the differential seismic slowness (the differences between the current estimates and the new estimates) at the  $i$ th location in the model. Given measurements of the traveltimes, a method for forward modelling through the current slowness model and a method for computing the partial derivatives, eq. (1) can, in principle, be solved for the differential slownesses.

Ray theory is usually used to forward model the arrival times and to compute the partial derivatives, but some codes are more sophisticated than others. Ray tracing methods may or may not correctly account for ray curvature in the current model. The generation of the partial derivatives can be simplified in the case of straight ray segments (Dyer and Worthington, 1988). In the more correct, curved ray case quite complex analytical expressions are required (Bregman et al., 1989a).

In practical crosshole applications, eq. (1) is underdetermined (there are an infinite number of solutions that can fit a given data set). Furthermore, no data set is free of noise. In order to manage the solution of underdetermined versions of eq. (1) in the presence of noisy data, care must be paid to the way in which the problem is constrained. Many algorithms for constraining, or regularizing, the inverse problem have been proposed.

The solution of eq. (1) can only be considered to be a single iteration in the solution of a non-linear problem. The partial derivatives are themselves a function of the solution, and traveltime tomography algorithms must recompute the differential travel times and the partial derivatives following each solution of eq. (1). There is no guarantee of convergence in such a scheme, although in practice non-linearity in tomography would appear to be weak enough that the iterative method converges (Bregman et al., 1989a).

Algorithms for traveltime tomography differ in forward modelling tech-

niques, in the computation of the partial derivatives, in the regularization used to solve eq. (1), and in the way in which non-linearity is handled. In this study, the methods used by Dyer and Worthington (1988), and Dyer (1988) were applied. Since the model in this study is comprised of homogeneous segments, we were able to accurately trace rays through the model using rays that consisted of straight segments within layers, and correct ray bending at interfaces. (The a priori knowledge of the nominal velocities and the geometries of the interfaces was used. The objective of our study was not to extoll the virtues of the particular implementation of travelttime tomography used, but rather to provide a result that would be representative of the best possible tomographic inversion).

### *Inverse generalized Radon transform (inverse GRT)*

Using diffraction-time curves to interpret seismic waveforms is a geometrical approach that was extensively used before the advent of the digital computer (see Hagedoorn, 1954). In the early 1970's this approach was developed into an algorithm for digital migration, a method we shall refer to as to diffraction-stack migration. The method is straightforward and intuitively obvious; for each image location a diffraction-time curve is computed, representing the arrival times of all scattered events in the data originating from that image location. Data are then summed over the curve; any scattered data from that image location sum coherently, all other data are discriminated against. The procedure is repeated for all image locations.

The diffraction-stack procedure was recognized by French and others (French, 1974; Schneider, 1978) as a solution to the Kirchhoff integral formulation of the wave equation in homogeneous media, provided the data were appropriately weighted and filtered before stacking. Beylkin (1985) showed how the solution to the seismic inverse problem in more general media could also be formulated as a weighted diffraction stack. This approach, based on Beylkin's earlier formulation (1984) of a generalized Radon transform and its inverse, was further developed and applied by Miller et al. (1987). [It should be noted that Beylkin's generalization of the Radon transform is not the same as Chapman's earlier (1981) generalized Radon transform].

The GRT associates each data point in time with an isochron surface passing through the perturbations. Dually, the inverse GRT associates each image point with a diffraction-time surface passing through all the records. [Hagedoorn (1954) referred to isochrons as curves of "maximum concavity" in the model and to diffraction-time curves as curves of "maximum convexity" in the data]. The inverse GRT is based on the Born linearization of the acoustic wave equation. Algorithmically, the inverse GRT differs primarily from other migration techniques in the form of the "obliquity factor", dependent on the angle between incident and diffracted rays at a given image point.

Most migration operators contain an obliquity factor (the exception is diffraction-stack migration which contains no weighting, filtering or obliquity factor). In the inverse GRT the obliquity factor has been shown by Esmersoy and Miller (1989) to have an important effect, sharpening the point spread function (the image obtained from the data from a point scatterer). However, the obliquity factor can have a detrimental effect when the data contain a forward scattered component (i.e., the scatterers affect the arrival times). This deficiency of the inverse GRT arises because the Born approximation does not adequately model the transmitted wave through a scattering medium (a better approximation would be the Rytov approximation, see for example Slaney et al., 1984).

The diffraction-time curves are always tangent to the direct arrival curve at some point. Thus, if not removed, the high-amplitude direct wave field will contribute to the image at all points of the model. The obliquity factor referred to above in fact acts to discriminate against the direct arrival, although, especially for band limited data, the direct arrival will still contribute to the image. This is a manifestation of the corrupting effect of the direct wave field described in the Introduction. As with any wave-equation technique, it is necessary to separate the direct wave field from the total recorded wave field before applying the inverse GRT. This pre-processing stage is further described in the Results section.

The inverse GRT requires extensive ray tracing in order to generate the appropriate diffraction-time curves. The ray tracing is most efficiently carried out by computing and storing a table of times for each image location, corresponding to the times for ray paths to the image point, (i) from each source location, and (ii) from each receiver location. The time of a diffracted arrival for a particular source and a particular receiver is simply the sum of the two times. For the purposes of this paper, the traveltimes tables were computed by ray tracing, using the velocities from traveltimes tomography. Ray paths were refracted at model interface locations in the same manner as in the tomographic velocity imaging.

An important aspect of the inverse GRT is that the point spread function is intimately related to the range of the angles of the isochron surfaces available. Where only a limited set of isochron surfaces are available (for example, from data from a single source position), the point spread functions spread along the isochron surfaces. This fact can be utilized in incorporating a priori information about the prevailing range of dip angles. By limiting the local dips of the actual isochron surfaces to conform with this a priori information, better resolved images are obtained. This approach was used by van der Poel and Cassell (1989) in imaging single offset VSP data, who referred to this as a "dip aperture". Here we implemented a dip aperture by not stacking data when the computed angle between incident and diffracted rays was greater

than 120 degrees (for a given incident ray and imaging point, this rejects higher dip data).

Application of the method to crosshole data differs slightly from surface reflection data due to energy being diffracted from above, below and between each source and receiver pair, whereas only diffractions from below are present in surface reflection data. To account for these differences the polarity of energy diffracted from above a source and receiver pair was reversed before being stacked (cf. Hu et al., 1988). This was done by partitioning the data into positive and negative apparent velocity components by the application of an  $f$ - $k$  filter. Two images of the velocity discontinuities were formed; one from the upgoing events and one from the downgoing events. The polarity of one of the images was then changed before summing the two images.

### *Frequency-domain wave-equation imaging*

The frequency-domain wave-equation imaging technique used here has been described fully elsewhere (Pratt and Worthington, 1990; Pratt, 1990a, b; Pratt and Goult, 1991). The imaging technique is derived from a gradient method for wave-equation inversion (Tarantola, 1984a, b). The most important aspect of Tarantola's work was the derivation of a tractable algorithm for calculating the gradient of an objective function with respect to perturbations in the acoustic (or elastic) parameters of the medium. The objective function is used to quantify the misfit of the current model. The gradient of the objective function is the direction of steepest descent in the model space and, as such, can be displayed as an image of the model errors. If one begins with a smooth version of the true velocities, the image will depict the discontinuities in the velocities.

Tarantola formulated the inverse problem in the time-space domain. Others have used the frequency-wavenumber domain (Stolt, 1978; Devaney, 1984; Wu and Toksöz, 1987). In the context of crosshole seismics, an implementation in the frequency-space domain is perhaps most appropriate (Woodward and Rocca, 1988). Provided the survey aperture is wide, there is a greater redundancy in the information content of the recorded wave field. Useful images can be formed from single frequency components of the data, and image enhancement can be implemented by simply summing as many images from separate frequency components as may be required. Either the acoustic wave equation or the elastic wave equation can be used. Best results are obtained using the elastic wave equation, although this is achieved only at considerable additional computational expense. In this paper we use the gradient method for elastic wave-equation imaging, implemented in the frequency-space domain (see Pratt, 1990a). The images we show were formed by summing the images from five individual frequency components of the data.

An important aspect of the gradient approach to wave-equation inversion is the lack of any dependence on particular forward modeling algorithm. The method only requires some method for propagating waves, the user is free to decide which method is appropriate for a particular application. In the context of multiple source cross hole seismics an appropriate technique is the method of finite differences, applied in the frequency domain (Pratt, 1990b). The computational efficiency of frequency-domain finite differences complements the frequency-domain approach to imaging.

The imaging method operates on only a single frequency component of the data at a time. Mono-frequency scattered wave fields for each source position are time reversed and used as forcing functions in a wave propagation stimulation. A partial image for each source is formed by multiplying these “back-propagated” data by a second wave field, computed by forward propagating the source terms. Before multiplication, an “adjoint operator” is applied to both wave fields. The adjoint operator acts to unravel the wave field information into the desired model parameter, in this case velocity anomalies (Mora, 1987). The multiplication of the two frequency-domain wave fields is equivalent to the application of an imaging condition; it replaces the cross-correlation of time-domain wave fields performed in many time-domain migration or inversion algorithms. Following the computations of the partial images for each source position, the results are summed from all 51 source positions to yield a final image.

## RESULTS

This section describes the results we obtained when we used the three methods described in the Algorithms section (above) to form images from the scale model data described earlier. The wave field pre-processing required for wave-equation imaging and results of pre-processing the model data are also described in this section.

### *Tomography*

First arrival times were picked on both the pre-flood data. We used these times to form velocity images by traveltimes tomography. As described in the introduction, the ray paths used in this study were obtained by ray tracing through an interface model based on Fig. 1 (the nominal velocities were used to compute ray bending at interfaces). We used this approach in order to simulate the optimal performance of a curved ray tomography algorithm.

The “true” ray paths described above were used to form the tomograms from the pre-flood data (Fig. 3a) and the post-flood data (Fig. 3b). The solution of eq. (1) was accomplished using the simultaneous iterative reconstruction technique (SIRT) (Dines and Lytle, 1979). Eleven iterations of the

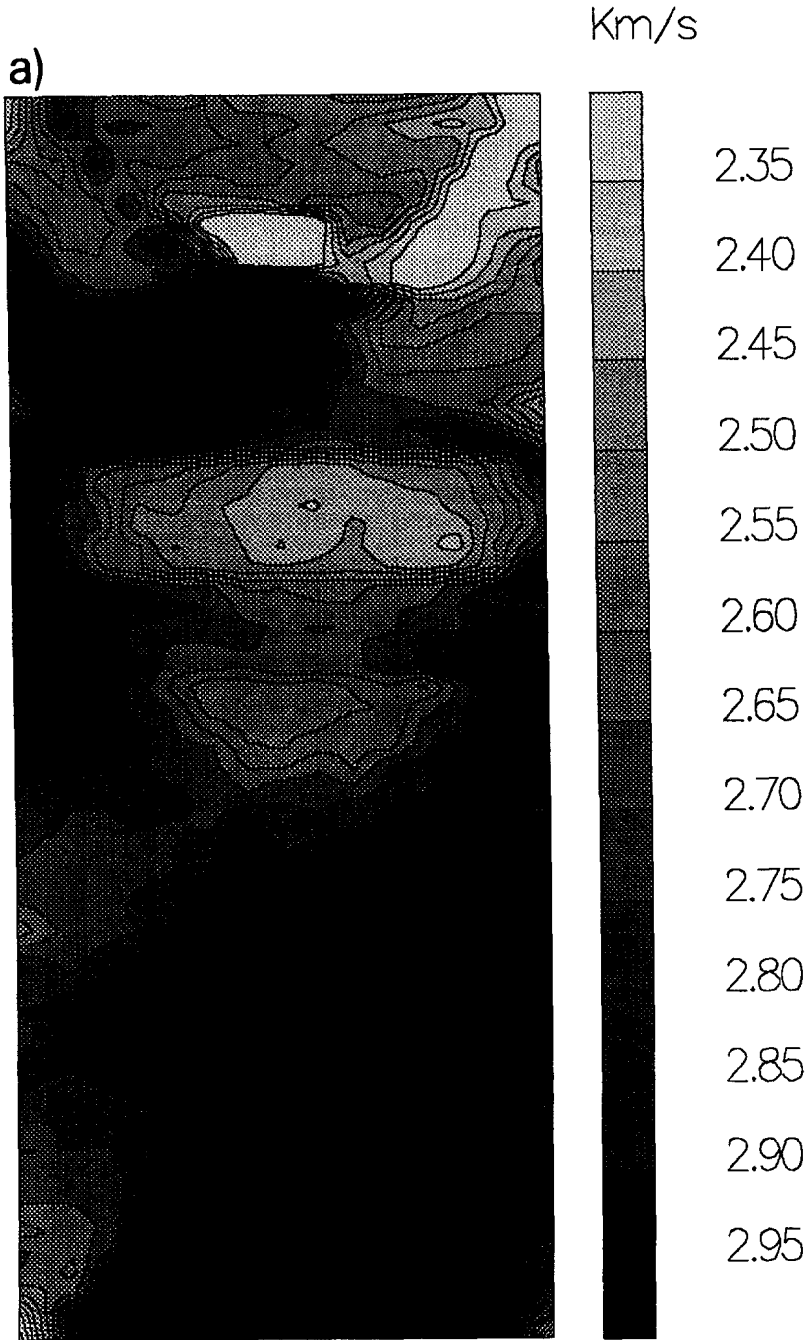
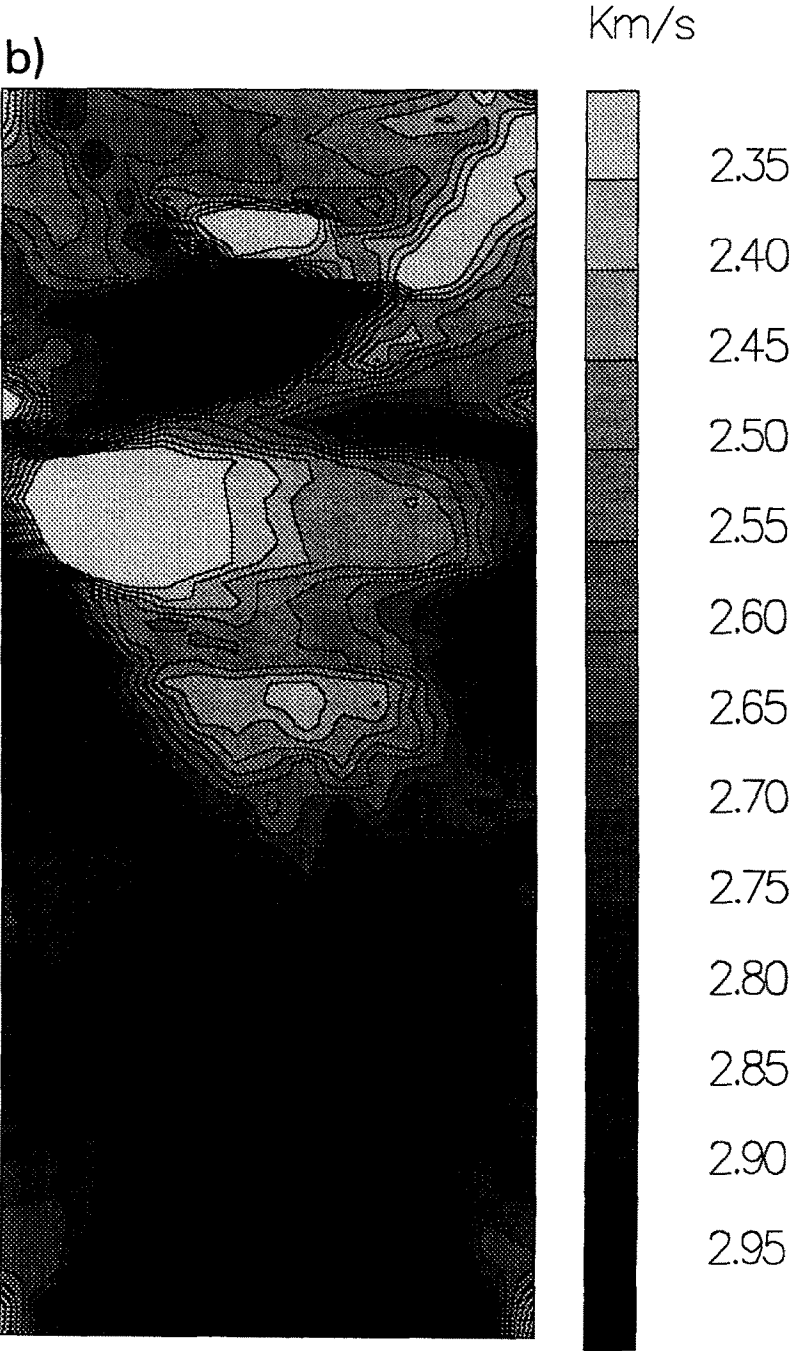


Fig. 3. Traveltime tomography results (compressional velocity maps). (a) Tomography image from the pre-flood data, (b) tomographic image from the post-flood data, and (c) differences between pre-flood and post-flood tomography results. The image dimensions are the same as those given in Fig. 1.



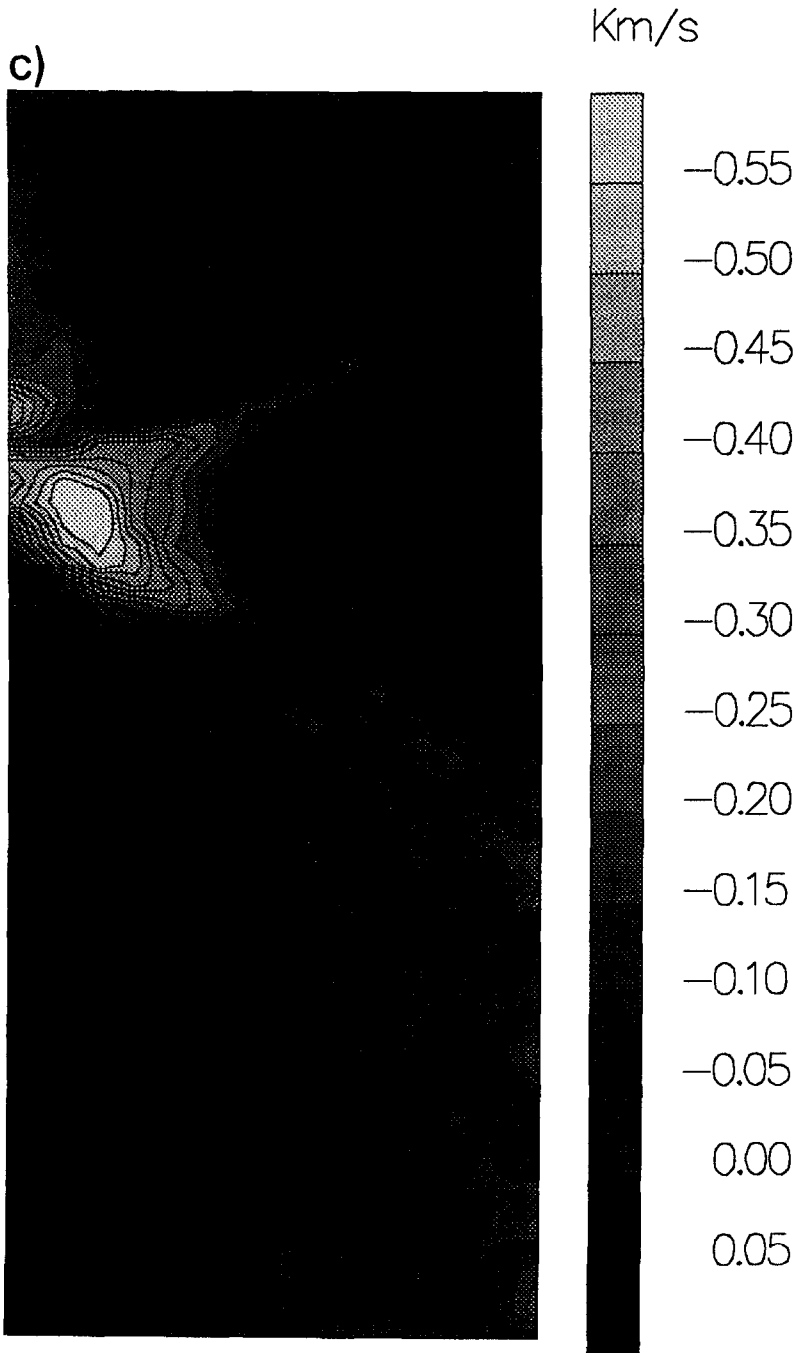


Fig. 3. (Continued).

SIRT were used in both cases. Figure 3c shows the difference image obtained by subtracting the two velocity images from each other. The presence and position of the flood zone can be easily discerned, although the exact geometry of the flood “front” cannot be interpreted from these images. The differences in velocities introduced by the presence of the flood zone can be estimated from these results to be of the order of 0.4 km/s. This is much larger than the difference in the nominal velocities (0.016 km/s). It should be noted that the true velocities can differ from the nominal velocities due to local factors in the preparation of the epoxy resins for the model (for example, the absorption of water from the ultrasonic tank).

The same ray paths were used in the formation of both the pre-flood and post-flood images. These ray paths were based on the nominal velocities, without the presence of the flood zone. The magnitude of the velocity perturbation due to the flood zone was greater than was expected when the model was designed, and some of the artifacts that can be seen on the difference image are due to the inaccuracies of the ray paths in the post-flood inversion. An iterative, curved ray approach could likely have reduced the effect of these artifacts.

Tomographic image resolution is essentially governed by two factors. The first of these is the Fresnel zone width associated with the wave propagation. Traveltimes are unaffected by variations within a Fresnel zone width. The Fresnel zone has dimensions of the order of  $\sqrt{L\lambda}$  (see, for example, Williamson, 1991), where  $L$  is the propagation distance and  $\lambda$  is the wavelength. For this survey  $L \approx 55$  mm and  $\lambda \approx 7$  mm, so that the Fresnel zone width is of the order of 19 mm. The survey should be able to resolve anomalies provided they are, say, half this distance apart, or approximately 10 mm. Our results appear to have a better resolution than this, partly due to the fact that the ray paths were fixed, a priori, by the nominal velocities. The central layer (2.81 km/s, 8.5 mm thick) is just barely resolved.

The second factor governing resolution is the smoothing imposed by the particular linear equation solving technique used. Because tomography, for borehole geometries, results in extremely ill-conditioned systems, overfitting of data can result in the amplification of noise (picking errors) and unreasonable images. This is avoided by solving only for the well determined model eigenvectors (in practice this can be achieved limiting the number of iterations of SIRT). Because the well determined eigenvectors correspond approximately to the smooth components of the model (see for example, Bregman et al., 1989c) the images are at least as smooth as the roughest eigenvector used. This smoothness is very difficult to quantify as it depends critically on factors such as the number of sources and receivers, the aspect ratio of the survey and the noise level of the data. However, it is likely that the smoothness imposed by the solution method is within the Fresnel zone width quoted above.

### *Wave field pre-processing*

In order to proceed to processing of the wave fields using the inverse GRT and the frequency-domain wave-equation imaging methods, it was necessary to pre-process the data. This involved two stages. In the first stage an estimate of the direct wave field was obtained and used to deterministically deconvolve the data. In the second pre-processing stage the deconvolved data were separated into direct and scattered (deconvolved) wave fields. This method of obtaining an input to wave-equation imaging schemes, if carefully applied, works well with good quality field data.

The separation of downgoing (direct) wave fields from the upgoing (scattered) wave fields is a standard procedure that is regularly applied to vertical seismic profile (VSP) data. Similarly, in processing VSP data the downgoing wave field is often used to design deterministic deconvolution operators. Using techniques very similar to those used in VSP processing, we applied a moveout correction to align neighbouring traces according to their first arrival times, and then applied a running mean filter (as described in Hardage, 1983) to form an estimate of the direct arrival. In order to discriminate against scattered waves that might have similar moveouts to the direct waves, the running mean was applied in both common source and common ray angle domains. This modification, first described by Pratt and Gouly (1991), is essential in order to effectively separate direct and scattered wave fields in crosshole applications.

The purpose of the first pre-processing stage, deconvolution, was twofold. Firstly, to compress the source wavelet, since wavelet compression is required for the inverse GRT to perform well. Secondly, it was desirable to remove the coherent variation in the source signature with ray angle. A different deconvolution filter was computed at each ray angle, and used to deconvolve all the data with a common ray angle to a globally consistent wavelet. (Just here, the term ray angle is used to refer to the angle between the horizontal and a straight line joining source-receiver pairs.) The post-flood data following deconvolution are shown in Fig. 4a.

In the second pre-processing stage a scattered wave field was estimated from the deconvolved data. In the absence of pre-flood data this is the only way of obtaining a suitable input to the full waveform schemes. The direct wave field was extracted from the deconvolved data in the same manner as described above. In this case, the direct wave field was then subtracted from the total deconvolved wave field to yield the deconvolved scattered wave field. Because direct shear waves were also present, these were also removed in a similar fashion, by using moveout corrections based on picked shear wave arrivals. A common receiver gather of the data following the removal of both direct wave types is shown in Fig. 4b.

In the pre-processing of data for the frequency-domain imaging we left scat-

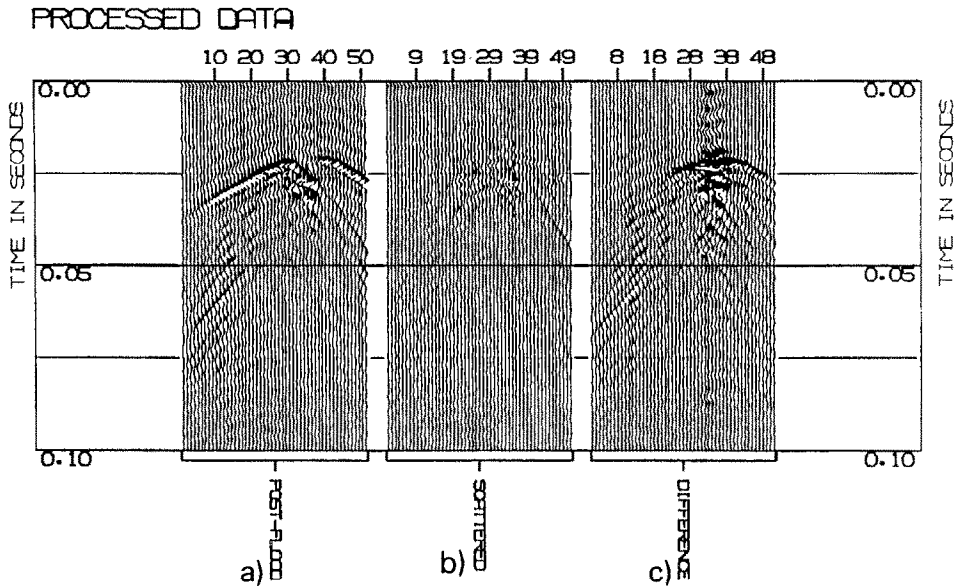


Fig. 4. Wave field pre-processing. (a) Deconvolved post-flood data. (b) Scattered wave field extracted from post-flood data in (a). (c) Deconvolved difference data. Numbers on the horizontal axes refer to the source numbers (see Fig. 1).

tered shear waves intact, a desirable effect since we applied an elastic wave equation algorithm, which backpropagates both shear and compressional scattered waves simultaneously. For the inverse GRT we also attempted to remove remaining, scattered or mode converted shear wave energy. This was accomplished by applying a recursive dip filter (Hale and Claerbout, 1983). A cutoff dip of 1.6 km/s was used in the recursive dip filter. (It should be noted that some reflected compressional waves may be attenuated using this approach.)

### *Difference wave fields*

Where a repeatable crosshole survey has been carried out before and after reservoir stimulation, a different, and more accurate (but less robust) approach can be used to eliminate the effects of the direct wave. In such cases the two data sets are subtracted from each other, providing a difference wave field. It is well known that such difference fields can be described to first order by the (distorted wave) Born approximation (see, for example, Aki and Richards, 1980). The use of the Born approximation allows the difference wave fields to be expressed as the solution to a new wave equation in which the parameter perturbations act as virtual sources. When applying migration-like techniques the imaging condition is satisfied at the locations of these vir-

tual sources. Therefore, the difference field is a suitable input to migration or imaging algorithms when one is interested in mapping the geometries of the altered velocity zones. The difference wave field, following the application of the deconvolution process described above, is shown in Fig. 4c.

### *Images from scattered wave fields*

An inverse GRT image and an elastic wave-equation image, both formed from the deconvolved, pre-flood, scattered wave field are shown in Figs. 5a and 5b. The extensive ray tracing required to generate the inverse GRT image took roughly 5 hours to perform on a VAX 11/780. As described above, ray paths were assumed to consist of straight segments — curved ray tracing would have taken much longer. Each wave equation image took 4 hours to compute on an FPS-164/MAX scientific computer. The image shown in Fig. 5b is the sum of five images obtained from five different frequency components of the scattered data, equally spaced within the temporal bandwidth of the data.

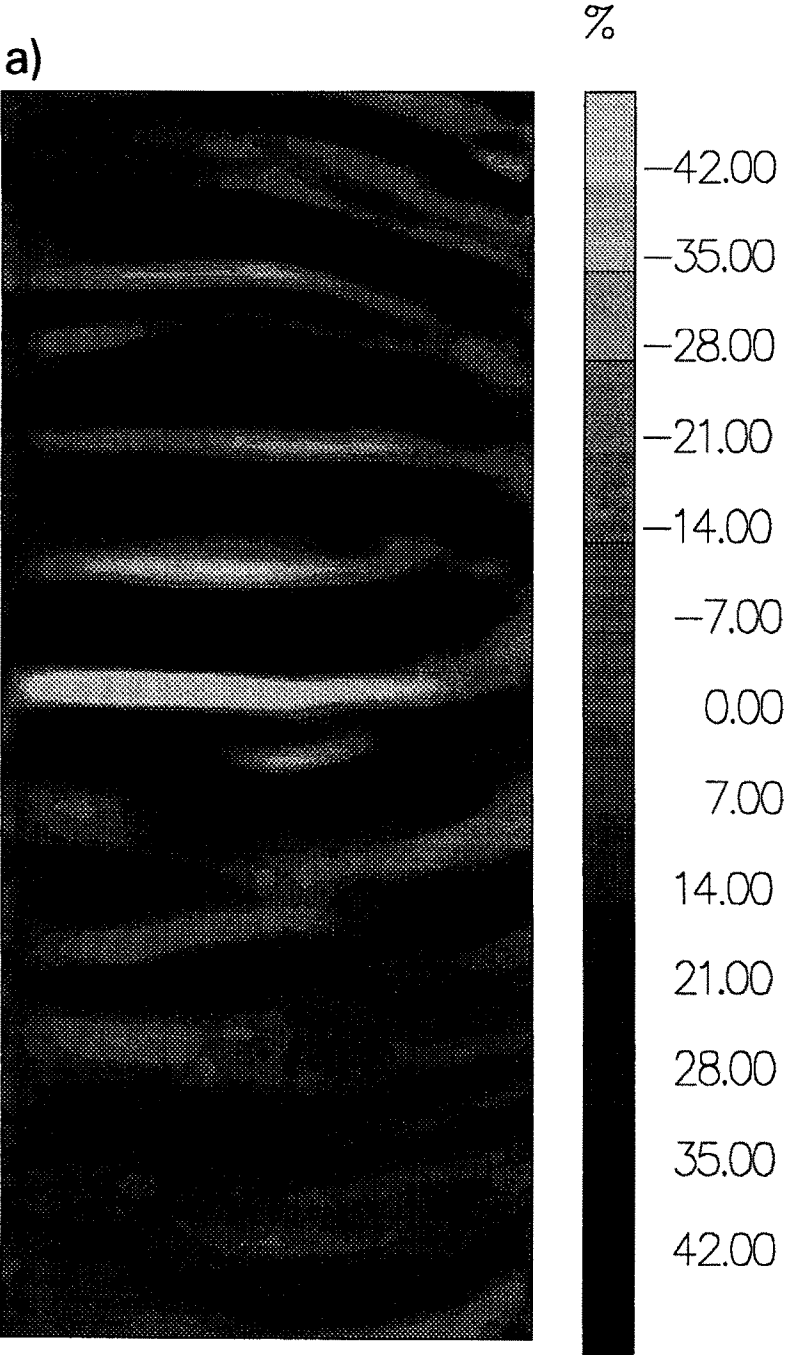
The two full waveform results (Figs. 5a and 5b) each have their own merits and deficiencies. In both images the interfaces are better defined than on the tomography image, Fig. 3a. The inverse GRT (Fig. 5a) yields an excellent image of the interfaces (i.e., the discontinuities in the velocities). The high-amplitude “events” on this image all correspond to real interface locations in the model. In contrast, the wave-equation image, Fig. 5b, is not as well focussed. The dipping layer, and the vertical fault, are better recovered in the inverse in the GRT image. However, the wave-equation image has succeeded in recovering a better image of the semi-circular channel feature at the center of the model.

The differences described in the paragraph above can be understood in terms of the physical basis of each of the algorithms. The inverse GRT is a true linearized inversion. The obliquity factor (discussed in a previous section) ensures that, in linear problems (i.e., where the starting model is close to the true model), the result will be an exact image of the errors in the model. As stated in the Introduction, the wave-equation technique requires iteration, even in linear problems. Thus we expect that the inverse GRT will yield a better focussed result over most of the model.

In contrast to the inverse GRT, the wave-equation method uses the method of finite differences, rather than ray theory, to model wave propagation. In

---

Fig. 5. Images from scattered wave fields (as in reflection seismic images, the units of these images are meaningless). (a) Inverse GRT image using pre-flood scattered data. (b) Elastic wave-equation image formed by stacking separate results from five frequency components of the pre-flood scattered data. (c) Image formed by subtracting two inverse GRT images (the pre-flood and the post-flood images) from each other. Images in (a) and in (b) have been normalized to  $\pm 50\%$ . The image in (c) has the same normalization factor as in (a). The image dimensions are the same as those given in Fig. 1.



b)

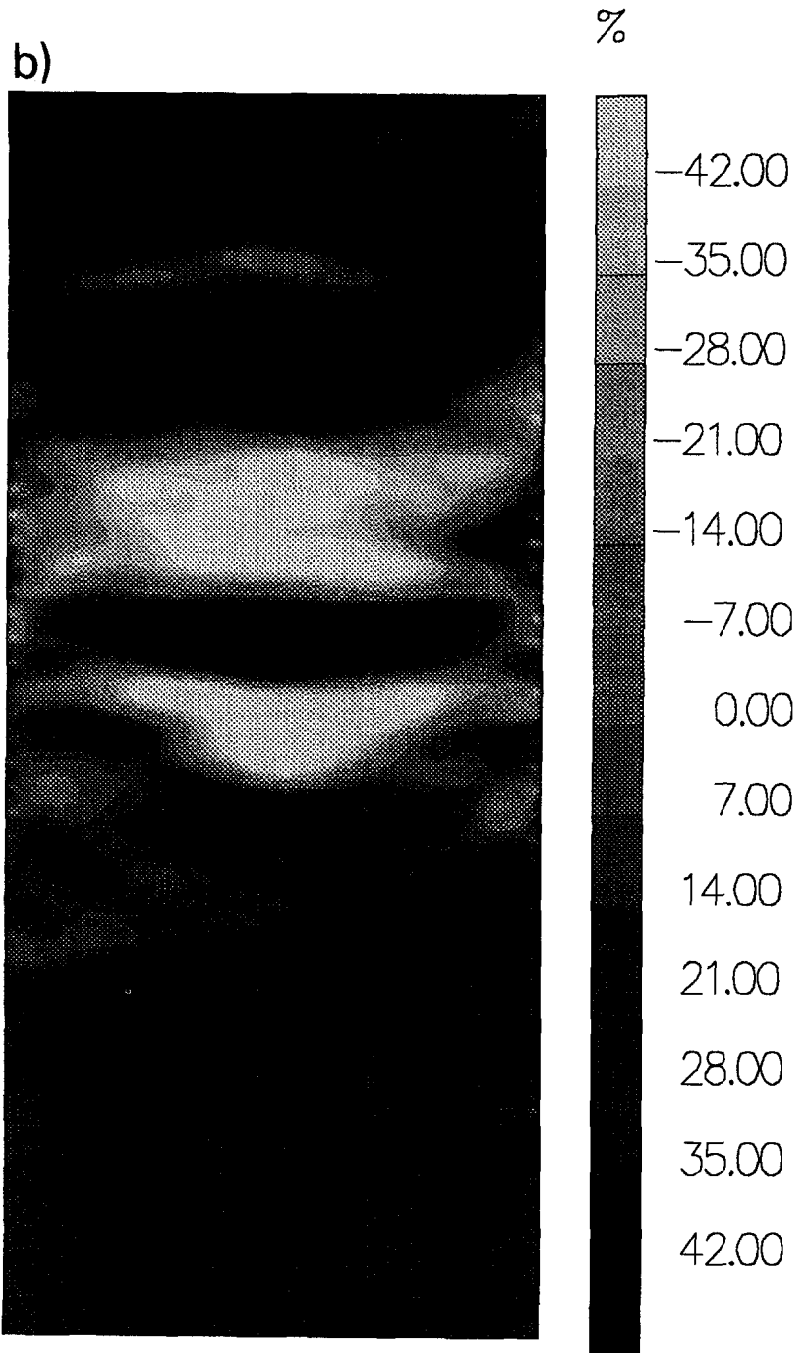
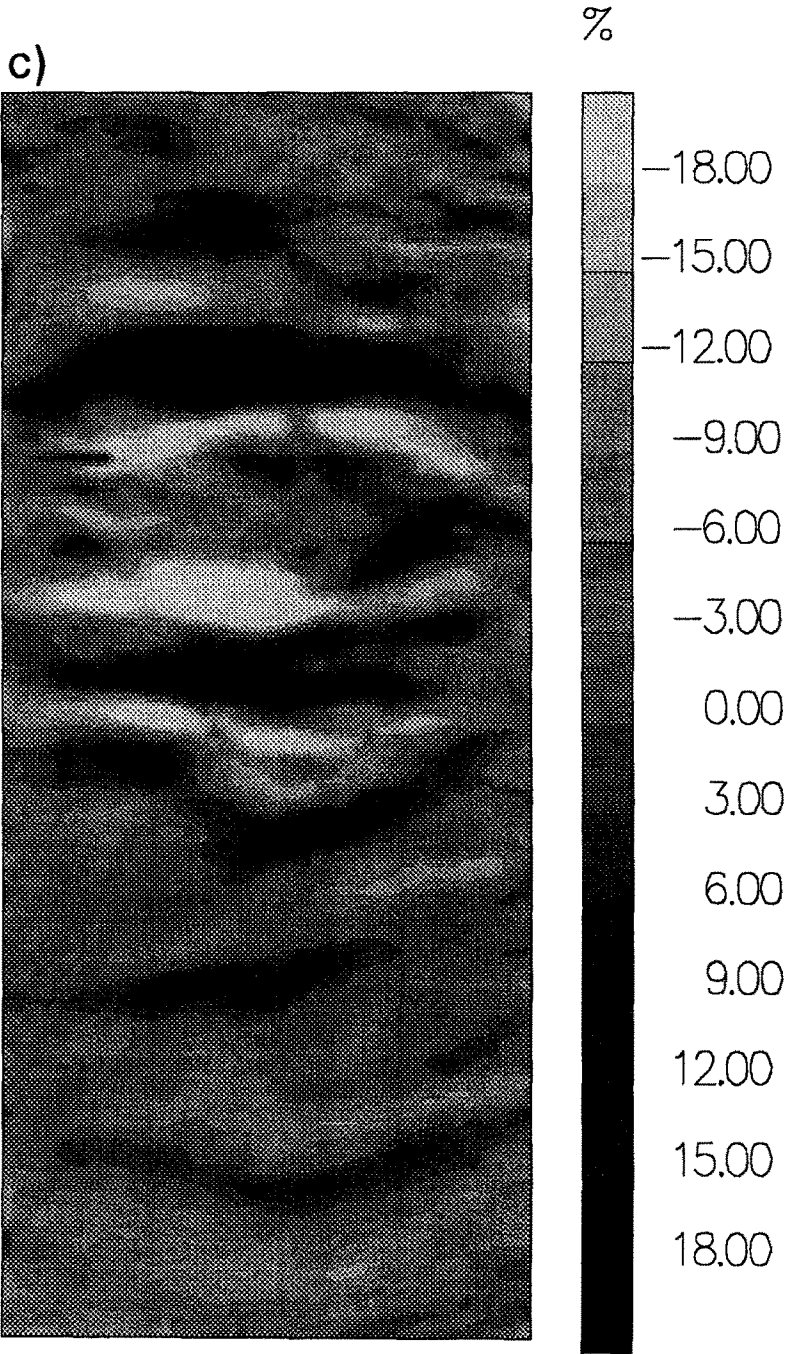


Fig. 5. (Continued).



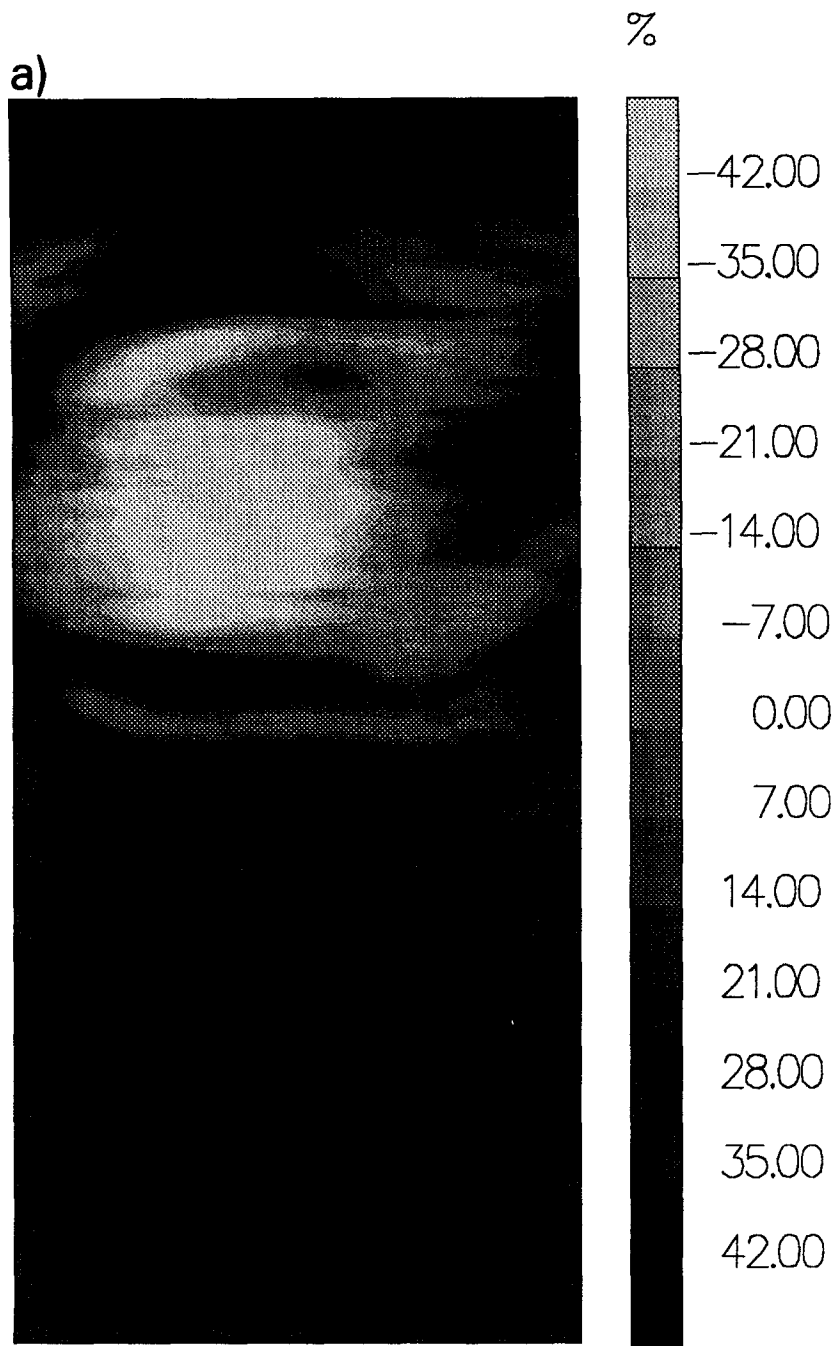
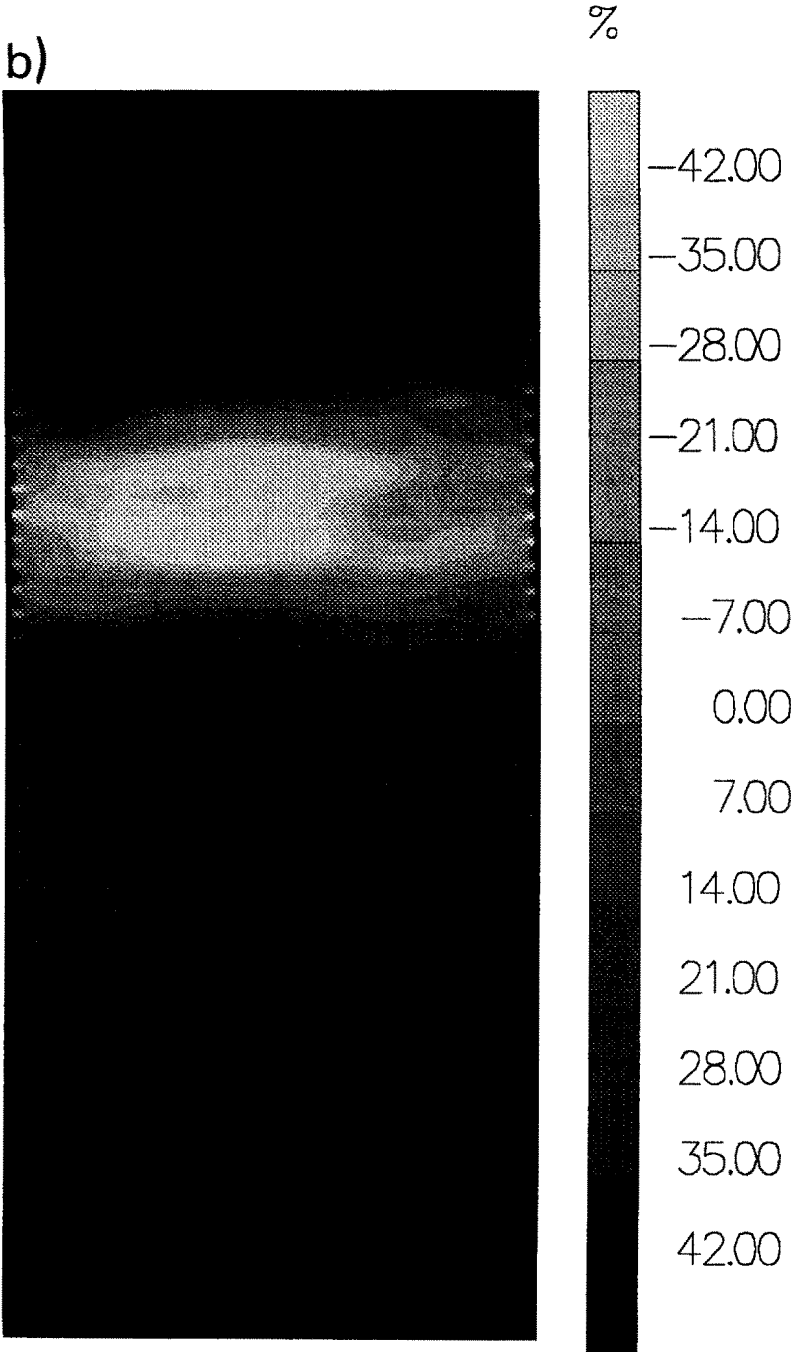


Fig. 6. Images from difference wave fields. (a) Diffraction-stack migration of difference wave field. (b) Elastic wave-equation image formed by stacking separate results from five frequency components of the difference wave field. Images in (a) and in (b) have been normalized to  $\pm 50\%$ . The image dimensions are the same as those given in Fig. 1.



regions of high model complexity, such as at the central channel feature, it proved difficult to find solutions to the ray equations. The finite difference method encounters no such difficulties. The finite difference solution also succeeds in modelling the trapped, or guided wave modes that exist in the two low velocity layers. These guided waves can be clearly seen in the raw data (see the central traces in Fig. 2a). Thus, we can understand that wave-equation imaging yields a superior image of the channel feature.

The inverse GRT was also used to form an image from the post-flood scattered data. (For reasons associated with the cost of computing time these data were not used to form a wave-equation image.) The same ray paths were used for the ray tracing of both pre-flood and post-flood models; in the former case the times were modelled by integrating slownesses from the pre-flood tomogram (Fig. 3a) over the ray paths, in the latter case the slownesses from the post-flood tomogram were integrated. As in the tomography, additional aberrations were created by ignoring the effects of the flood zone on the ray paths.

In Fig. 5c we show only the differences between the pre-flood GRT image and the post-flood GRT image. These differences represent changes in the magnitudes of the velocity discontinuities due to the presence of the flood zone. The flood zone can be seen to have altered the magnitudes of the velocity discontinuities above and below the zone. However, these images of these edges of the flood zone are associated with artifacts that “leak” into the layers above and below the flood zone and make the result very difficult to interpret. This leakage is a result of applying an incorrect imaging condition to the guided wave events arising from multiple internal reflections inside the reservoir layer — a manifestation of the inaccuracy of the acoustic ray approximation employed by the inverse GRT. The dipping interface between the flood zone and the reservoir layer is not recovered using this approach.

In contrast to tomographic imaging, the scale length that governs the resolution of a wave-equation image is not the Fresnel zone width, but the wavelength (approximately 7 mm in this survey). If the aperture of the survey were sufficiently wide and the noise level sufficiently low, we would hope to be able to resolve anomalies as close as, say, a half wavelength apart (3.5 mm). The fact that the layer containing the semi-circular anomaly can be seen on these images even at its thinnest portion (3 mm) suggests that this is a fair measure of the resolution. The wave equation images are significantly better resolved than the tomography images.

### *Images from difference wave fields*

The final images of this paper are an inverse GRT image (Fig. 6a) and an elastic wave-equation image (Fig. 6b), both formed using the deconvolved difference wave fields (Fig. 4c) as input data. Because the flood zone acts as

a virtual source for the difference fields, we expect the images to effectively map the flood zone. Both the images do in fact appear to yield quite satisfactory images of the actual areal extent of the flood zone. These are both an improvement on the results obtained from the scattered data (Fig. 5c) and a great improvement on the travelttime tomography results, Fig. 3c.

The differences in these images reveal much about the algorithms. The first point to be made is that the image in Fig. 6a was obtained by suppressing the obliquity factor in the inverse GRT (thus we refer to it as a diffraction-stack image). When the obliquity factor was included, the image looked similar to Fig. 5c. This is because the obliquity factor has the effect of reducing the weight of data lying close to the direct arrival curve (since this is where the angle between incident and diffracted rays is greatest). Yet, data close to the direct arrival curve is critical in the difference data. This high amplitude data (see Fig. 4c) is primarily due to the differences in the arrival time of the direct and refracted body waves. We conclude that these data contribute importantly to the image of the flood front, and that the inverse GRT is better able to use these events without the obliquity factor. The Born approximation is known to be inadequate in describing arrival time perturbations, so that this effect is likely due to use of the Born approximation in the formulation of the inverse GRT.

The wave-equation image, Figure 6b, is our best image of the flood front. The finite difference propagation technique used has succeeded in confining the re-focussed wave fields to within the reservoir layer, whereas the inverse GRT has allowed the energy to leak into the layers above and below. In this case the more accurate modelling method of finite differences has overcome the advantages of using a linearized scheme such as the inverse GRT.

## CONCLUSIONS

Our primary conclusion is that crosshole seismic surveys are well suited to the EOR mapping problem. We believe our results show that the full waveform should be utilized in these applications. Travelttime tomography is an important step in forming maps of velocity distributions, but we emphasize that much more can be obtained from crosshole seismic data. The resolutions of the wave-equation images we obtained are almost twice as good as the resolution of the travelttime tomography images. However, since each wave-equation method is based on approximate methods, a thorough understanding of the physical basis of each method is critical in interpreting the images.

Inverse GRT imaging and wave-equation imaging using a finite difference approach each have their own strengths and deficiencies. Our results indicate that when the geology is relatively simple, an inverse GRT approach should yield well focussed images of the velocity discontinuities (geological interfaces). In complex regions and when multiply scattered arrivals are observed

(such as interbed multiples and guided waves), an approach based on finite difference modelling is more appropriate. The use of finite difference modelling can, of course, imply a considerable increase in the cost of computing images.

We have also compared EOR maps formed using scattered wave fields (extracted from a single recorded wave field) and difference wave fields (extracted by subtracting pre-stimulation data from post-stimulation data). We conclude that the latter approach yields the better images. We emphasize the importance of carrying out a repeatable survey, using identical survey geometries, if this approach is to succeed. Where operational constraints preclude this, we are reduced to pre-processing to extract a scattered wave field.

The scale model has clearly not simulated all the potential vagaries of field crosswell data. For example, borehole waves ("tube waves") are often a significant component of recorded wave fields. Although tube waves carry information, from the point of view of the algorithms discussed here they must be considered as a form of coherent noise and dealt with accordingly. Source and receiver coupling inconsistencies will also severely handicap the wave-equation approach. Finally, the ubiquity of anisotropy in the Earth's crust will cause very severe image distortions for both tomography and wave-equation imaging if not accounted for. Further research is certainly required to evaluate the severity of these problems and to attempt to find solutions.

The full waveform algorithms we have utilized to form the images for this paper operate on the scattered waves in the data. It is the signal to noise ratio of the scattered waves that will be critical when applying these methods to field data. Data adequate for traveltime tomography is not necessarily adequate for full wave from processing. The amplitudes of the scattered energy may be many decibels down from the directly arriving energy. Source and receiver coupling problems may not be a problem for traveltime measurements, but must be avoided when considering wave-equation methods. The immediate task at hand is to obtain suitable datasets for the field evaluation of the methods outlined in this paper.

## REFERENCES

- Aki, K. and Richards, P.G., 1980. *Quantitative Seismology, Theory and Methods*. Freeman, New York.
- Beydoun, W.B., Delvaux, J., Mendes, M., Noual, G. and Tarantola, A., 1989. Practical aspects of an elastic migration/inversion of crosshole data for reservoir characterization: A Paris basin example. *Geophysics*, 54: 1587–1595.
- Beylkin, G., 1984. The inversion problem and applications of the generalized Radon transform. *Comm. Pure Appl. Math.*, 37: 579–599.
- Beylkin, G., 1985. Imaging of discontinuities in the inverse scattering problem by inversion of a causal generalized Radon transform. *J. Math. Phys.*, 26: 99–108.

- Bois, P., La Porte, M., Lavergne, M. and Thomas, G., 1971. Essai de détermination automatique des vitesses sismiques par mesures entre puits. *Geophys. Prospect.*, 19: 42–83.
- Bregman, N.D., Hursley, P.A. and Chapman, C.H., 1989a. Crosshole seismic tomography. *Geophysics*, 54: 200–215.
- Bregman, N.D., Bailey, R.C. and West, G.F., 1989b. Seismic tomography at a fire flood site. *Geophysics*, 54: 1082–1090.
- Bregman, N.D., Bailey, R.C. and Chapman, C.H., 1989c. Ghosts in tomography: the effects of poor angular coverage in 2-D seismic travelttime inversion. *Can. J. Expl. Geophys.*, 25: 7–27.
- Chang, W.F. and McMechan, G.A., 1986. Reverse time migration of offset vertical seismic profiling data using the excitation-time imaging condition. *Geophysics*, 51: 67–84.
- Chapman, C.H., 1978. A new method for computing synthetic seismograms. *Geophys. J.R. Astron. Soc.*, 54: 481–518.
- Chapman, C.H., 1981. Generalized Radon transforms and slant stacks. *Geophys. J.R. Astron. Soc.*, 66: 445–453.
- Devaney, A.J., 1984. Geophysical diffraction tomography. *Trans. Inst. Electr. Electron. Eng.*, GE-22: 3–13.
- Dines, K.A. and Lytle, R.J., 1979. Computerized geophysical tomography. *Proc. Inst. Electr. Electron. Eng.*, 67: 471–480.
- Dyer, B.C., 1988. Seismic reflection and transmission tomography. Ph.D. Thesis, University of London.
- Dyer, B.C. and Worthington, M.H., 1988. Some sources of distortion in tomographic velocity images. *Geophys. Prospect.*, 36: 209–222.
- Esmersoy, C. and Miller, D., 1989. Backprojection vs. backpropagation in multi-dimensional linearized inversion. *Geophysics*, 54: 921–926.
- French, W.S., 1974. Two-dimensional and three dimensional migration of model-experiment reflection profiles. *Geophysics*, 39: 265–277.
- Hagedoorn, J.G., 1954. A process of seismic reflection interpretation. *Geophys. Prospect.*, 2: 85–127.
- Hale, D. and Claerbout, J., 1983. Butterworth dip filters. *Geophysics*, 48: 1033–1039.
- Hardage, B.A., 1983. Vertical seismic profiling part a: Principles. Geophysical Press.
- Hu, L.-Z., McMechan, G.A. and Harris, J.M., 1988. Acoustic prestack migration of cross-hole data. *Geophysics*, 53(8): 1015–1023.
- Justice, J.H., Vassilou, A.A., Singh, S., Logel, J.D., Hansen, P.A., Hall, B.R., Hutt, P.R. and Solanki, J.J., 1989. Acoustic tomography for monitoring enhanced oil recovery. *Geophysics*, 8: 12–19.
- Kelly, K.R., Treitel, S. and Alford, R.M., 1976. Synthetic seismograms: a finite difference approach. *Geophysics*, 41(1): 2–27.
- Kretschmar, J.L., Kibbe, K.L. and Witterholt, E.J., 1982. Tomographic reconstruction techniques for reservoir monitoring. SPE 10990.
- Lo, T., Toksöz, M.N., Xu, S.-H. and Wu, R.-S., 1988. Ultrasonic laboratory test of geophysical tomographic reconstruction. *Geophysics*, 53: 947–956.
- McMechan, G.A., 1983. Seismic tomography in boreholes. *Geophys. J.R. Astron. Soc.*, 74: 601–612.
- Miller, D.E., Oristaglio, M., Beylkin, G., 1987. A new slant on seismic imaging: migration and integral geometry. *Geophysics*, 52: 943–964.
- Mora, P., 1987. Nonlinear two-dimensional elastic inversion of multioffset seismic data. *Geophysics*, 52: 1211–1228.
- Nur, A., 1982. Seismic imaging in enhanced recovery, SPE/DOE, 10680.
- Pratt, R.G., and Gouly, N.R., 1991. Combining wave-equation imaging with travelttime tomography to form high resolution images from crosshole data. *Geophysics*, 56: 208–224.

- Pratt, R.G. and Worthington, M.H., 1988. The application of diffraction tomography to cross-hole seismic data. *Geophysics*, 53(10): 1284–1294.
- Pratt, R.G. and Worthington, M.H., 1990. Inverse theory applied to multi-source cross-hole tomography. Part I: Acoustic wave equation method. *Geophys. Prospect.*, 38: 287–310.
- Pratt, R.G., 1990a. Inverse theory applied to multi-source cross-hole tomography. Part II: Elastic wave equation method. *Geophys. Prospect.*, 38: 311–330.
- Pratt, R.G., 1990b. Frequency-domain elastic wave modeling by finite differences: a tool for cross-hole seismic imaging. *Geophysics*, 55: 626–632.
- Schneider, W.A., 1978. Integral formulation for migration in two and three dimensions. *Geophysics*, 43: 49–68.
- Sharp, R.J., Peacock, J.H. and Gouly, N.R., 1985. Ultrasonic modelling system: Presented at the 47th Ann. Mtg., Eur. Assn. Expl. Geophys., Budapest.
- Slaney, M., Kak, A.C. and Larsen, L.E., 1984. Limitations of imaging with first-order diffraction tomography. *Trans. Microwave Theory and Technology, Inst. Electr. Electron. Eng., MIT-32*: 860–873.
- Stolt, R.H., 1978. Migration by Fourier transform. *Geophysics*, 50: 2458–2472.
- Tarantola, A., 1984a. Inversion of seismic reflection data in the acoustic approximation. *Geophysics*, 49: 1259–1266.
- Tarantola, A., 1984b. The seismic reflection inverse problem. In: F. Santosa, Y.H. Pao, W. Symes and Ch. Holland (Editors), *Inverse Problems of Acoustic and Elastic Waves*. Soc. Industr. Appl. Math.
- Toksöz, M.N., Cheng, C.H. and Timur Ayetikin., 1976. Velocities of seismic waves in porous rocks. *Geophysics*, 41: 621–645.
- Van der Poel, N.J. and Cassell, B.R., 1989. *Geophysics*, 54: 1091–1100.
- Wang, Z. and Nur, A., 1988. Effect of temperature on wave velocities in sands and sandstones with heavy hydrocarbons. *Soc. Pet. Eng. Res. Eng.*, 3: 158–164.
- Wayland, J.R. and Leighton, A.J., 1985. Mapping technology: a key to EOR control. *Oil Gas J.*, 109–115.
- Williamson, P., 1991. A guide to the limits of resolution imposed by scattering in ray tomography. *Geophysics*, 56: 202–206.
- Wong, J., Bregman, N., West, G. and Hurley, P., 1987. Cross-hole seismic scanning and tomography. *Geophysics*, 36–41.
- Woodward, M.J. and Rocca, F., 1988. Wave-equation tomography: Presented at the 58th Ann. Int. Mtg. Soc. Expl. Geophys., Anaheim, Ca., Expanded Abstr., pp. 1232–1235.
- Worthington, M.H., 1984. An introduction to geophysical tomography. *First Break*, 2: 20–25.
- Wu, R. and Toksöz, M.N., 1987. Diffraction tomography and multisource holography applied to seismic imaging. *Geophysics*, 52: 11–25.